



Article

Investigation of the Prospects for the Use of Iron-Containing Nanocomposites Doped with Rare Earth Elements as Catalysts for the Purification of Aqueous Media

Kayrat K. Kadyrzhanov ¹, Artem L. Kozlovskiy ^{1,2,*} , Kamila B. Egizbek ¹, Sholpan N. Kubekova ³, Inesh E. Kenzhina ^{3,4} and Maxim V. Zdorovets ^{1,5} 

¹ Engineering Profile Laboratory, L.N. Gumilyov Eurasian National University, Satpayev St., Astana 010008, Kazakhstan

² ASU Innovations, Kh. Dosmukhamedov Atyrau University, Studenchesky Ave., Atyrau 060009, Kazakhstan

³ Department of General Physics, Satbayev University, Almaty 050032, Kazakhstan

⁴ Advanced Electronics Development Laboratory, Kazakh-British Technical University, 59 Tole bi St., Almaty 050000, Kazakhstan

⁵ Department of Intelligent Information Technologies, Ural Federal University, 620075 Yekaterinburg, Russia

* Correspondence: kozlovskiy.a@inp.kz; Tel./Fax: +77-024-4133-68

Abstract: The great interest in nanostructured magnetic composites is due to their great prospects for use as a basis for the development of catalysts for the adsorption of manganese in wastewater. Interest in magnetic nanocomposites in this direction is primarily due to the possibility of extracting them from water media using ordinary magnets, which allows them to be used again. Additionally, it is worthwhile to note interest in research related to increasing the efficiency of adsorption, as well as an increase in the number of repeated cycles of operation. In this regard, the main goal of this study is to study the prospects for applying the method of mechanochemical synthesis for the creation of iron-containing nanocomposites doped by rare-earth elements Gd, Ce, Y, and Nd in order to obtain optimal catalysts for cleaning water media. During the studies, structural properties and phase composition of synthesized nanocomposites were established, as well as ultra-thin parameters of the magnetic field. It has been established that the kinetic curves of the adsorption process can be described by a pseudo-first-order model, and the process of manganese adsorption itself is associated with the cationic interaction of manganese ions with the surface of nanocomposites. The kinetic curves of degradation were determined, as well as the influence of the number of cyclic tests on the adsorption of manganese for synthesized nanocomposites, depending on the type of dopant and phase composition, respectively. Iron-containing nanocomposites doped with gadolinium and neodymium have been found to have the highest adsorption efficiency and corrosion resistance. Particular attention is paid to the study of the stability of storage of nanocomposites for a long time, as well as the preservation of their adsorbent properties in the purification of aqueous media. It has been determined that the modification of nanostructures with the help of rare earth compounds leads to an increase in resistance to degradation, as well as to the preservation of the efficiency of adsorption for 5–7 cycles in comparison with Fe₂O₃ nanoparticles, for which low resistance to degradation was observed.

Keywords: nanocomposites; heavy metal adsorption; purification of aqueous media; magnetic nanoparticles; iron oxide



Citation: Kadyrzhanov, K.K.; Kozlovskiy, A.L.; Egizbek, K.B.; Kubekova, S.N.; Kenzhina, I.E.; Zdorovets, M.V. Investigation of the Prospects for the Use of Iron-Containing Nanocomposites Doped with Rare Earth Elements as Catalysts for the Purification of Aqueous Media. *Magnetochemistry* **2023**, *9*, 87. <https://doi.org/10.3390/magnetochemistry9030087>

Academic Editors: Kamil Gareev and Ksenia Chichay

Received: 25 February 2023

Revised: 21 March 2023

Accepted: 21 March 2023

Published: 22 March 2023



Copyright: © 2023 by the authors. Licensee MDPI, Basel, Switzerland. This article is an open access article distributed under the terms and conditions of the Creative Commons Attribution (CC BY) license (<https://creativecommons.org/licenses/by/4.0/>).

1. Introduction

In the modern world, the problems of wastewater pollution products in production in the form of heavy metals and various organic dyes are the most acute and require immediate solutions [1,2]. Moreover, in most cases, traditional purification methods are not effective since the degree of pollution in some cases is very large [3], and the use of

modern developments in the field of textile industry production leads to the creation of dyes resistant to degradation that can withstand most traditional methods of their disposal and decomposition [4,5]. In this regard, in the past few years, much attention has been paid to the search for alternative methods of wastewater cleaning of pollution, including the possibility of using various adsorbents. Interest in this direction is primarily focused on the possibilities of effective cleansing by adsorption of charge or heavy metals, as well as their decomposition in the case of organic dyes [6,7]. Moreover, an important role is played by the possibility of reuse of such catalysts, as well as the search for obtaining them with a fairly low cost and ease of receipt. Additionally, with the prolonged operation of such catalysts, it is necessary to take into account the possibility of extracting them from water media without losing the weight of the adsorbent. In this regard, much attention in this direction, taking into account all requirements, is paid to magnetic nanostructural materials that are very promising for such purposes [8–10]. Firstly, nano-sized grains increase the adsorbing ability of the material due to the increased area of the specific surface, as well as the developed hierarchical structure of grains. Secondly, the magnetic properties of nanoparticles make it possible to extract their water using magnets, with minimal losses during extraction [11,12]. Additionally, the most important advantage of nanomaterials is the simplicity of their production. The synthesis of magnetic nanoparticles based on iron oxide is one of the most common methods for obtaining nanostructures using a chemical deposition. Furthermore, this method makes it possible to obtain isotropic nanoparticles in any amount [13–15]. Moreover, the simplicity of the preparation method makes it possible to obtain iron-containing oxide nanoparticles, which can subsequently be used as a basis for creating composite nanostructures by mixing them with other particles; applying various polymer, organosilicon, or metal coatings on them to create “core-shell” particles; or using thermal annealing to vary the size and phase composition of particles [16–19]. In this regard, the variety of different modification methods opens up even more opportunities for research in this direction and also increases the number of potential compositions for practical use. The combination of factors such as ease of manufacture; high purification efficiency; degradation resistance during long-term operation; the possibility of repeated use; and, most importantly, the possibility of scaling up and production in any required quantities make iron-containing nanoparticles one of the promising catalysts for the purification of aqueous media.

Based on the foregoing, the key aim of this study is to comprehensively study the prospects for the use of iron-containing nanoparticles modified with rare earth elements as adsorbents for the purification of aqueous media, as well as to determine the most effective nanocomposite for these purposes. Additionally, the main distinguishing feature of the work is the use of the simplest methods for obtaining modified iron-containing nanocomposites, including chemical precipitation of iron oxide, known as the cheapest way to obtain nanopowder on an industrial scale, and mechanochemical grinding and subsequent thermal annealing of iron oxide with rare earth elements, which makes it possible to obtain composite nanostructures with a high degree of structural and magnetic ordering.

2. Experimental Part

For the synthesis of iron-containing nanoparticles, the chemical elements $\text{FeCl}_3 \cdot 6\text{H}_2\text{O}$ and Na_2SO_3 were used. Chemical compounds $\text{Gd}(\text{NO}_3)_3$, Nd_2O_3 , CeO_2 , Y_2O_3 , and chemical purity of 99.95% were chosen as doping elements. All chemicals were purchased from Sigma Aldrich (Sigma, St. Louis, MO, USA).

Nanocomposites based on magnetic iron oxide nanoparticles, hematite (Fe_2O_3) doped with gadolinium, neodymium, cerium, and yttrium, were chosen as objects for research. The preparation of nanoparticles was carried out using a combination of various synthesis methods. The composites were based on iron-containing oxide nanoparticles obtained by chemical decomposition. Doping with rare earth elements was carried out in a stoichiometric ratio of 1:1. Doping was carried out by mechanochemical grinding followed by thermal annealing in a muffle furnace at a temperature of 800 °C for 5 h. Mechanochemical

grinding was carried out in a PULVERISETTE 6 classic line planetary mill (Fritsch, Berlin, Germany). Grinding of the original components was carried out at a grinding speed of 250 rpm for 30 min.

The morphological features of the obtained nanocomposites before and after the experiments on the adsorption of pollutants were studied using the method of scanning electron microscopy. A Jeol JSM-7500F scanning electron microscope (Jeol, Tokyo, Japan) was used to obtain images of the nanocomposites. To detail the corrosion processes and their effect on the amorphization of nanocomposites when they are kept in model solutions for a long time, we used the technique of obtaining high-resolution images using transmission electron microscopy, implemented on a Jeol JEM 1400Plus transmission electron microscope (Jeol, Tokyo, Japan).

Characterization of the phase composition of the studied samples of nanocomposites chosen as the basis for catalysts for the adsorption of heavy metals was carried out using the method of X-ray phase analysis. The phase composition was determined using the X-ray diffraction method implemented on a D8 Advance ECO powder diffractometer (Bruker, Berlin, Germany). Diffractograms were taken in the Bragg–Brentano geometry in the angular range $2\theta = 20\text{--}80^\circ$, with a step of 0.03° .

The structural ordering degree was estimated by approximating the obtained diffractograms with a set of pseudo-Voigt functions, followed by determining the contributions of diffraction reflections and background radiation.

The study of hyperfine parameters of the magnetic field depending on the composition of the obtained nanocomposites was carried out using the method of Mössbauer spectroscopy, which was implemented using an MS1104Em spectrometer (Rostov, Russia) in the constant acceleration mode with a triangular shape of the Doppler velocity of the source relative to the adsorber. Co^{57} in an Rh matrix was used as the radiation source. The Mössbauer spectra were processed using SpectrRelax software (Moscow State University, Moscow, Russia). The Mössbauer spectra were measured at room temperature $25 \pm 2^\circ\text{C}$.

The applicability of the selected nanocomposites as catalysts for the purification of aqueous media was assessed by the adsorption of manganese from aqueous solutions. Model solutions containing manganese were prepared for the experiments. The manganese concentration in the model solution was 50 mg/L, and the pH of the model solution was 5.5. To determine the efficiency of adsorption, we used the method of determining the optical density of manganese ions in a model solution before and after adsorption using the photometric method. The adsorption efficiency (q_e) of metal ions in equilibrium was estimated using expression (1) [20]:

$$q_e = \frac{(C_0 - C_e)V}{m} \quad (1)$$

where C_0 and C_e are the concentrations of manganese in the initial state and after adsorption, V is the solution volume, and m is the mass of nanoparticles.

This method of measuring the mass concentration of manganese in samples of natural, drinking, and wastewater allows for determining the concentration of pollutants in the environment, as well as evaluating the efficiency of adsorption. To determine the optical density, a photometric device, «Fluorat—02», was used.

Tests for the stability of maintaining the efficiency of adsorption were carried out by sequentially placing nanoparticles in an aqueous solution with subsequent adsorption of manganese. After adsorption, the magnetic nanoparticles were removed from the aqueous solution and placed in a new solution for the next adsorption experiment.

3. Results and Discussions

3.1. Morphological Features of the Synthesized Nanocomposites

To characterize the morphological features and determine the isotropy of the geometric shapes and sizes of the synthesized nanocomposites by mechanochemical grinding and

subsequent thermal annealing, we used the method of analyzing images obtained using the scanning electron microscopy method, the images of which are shown in Figure 1.

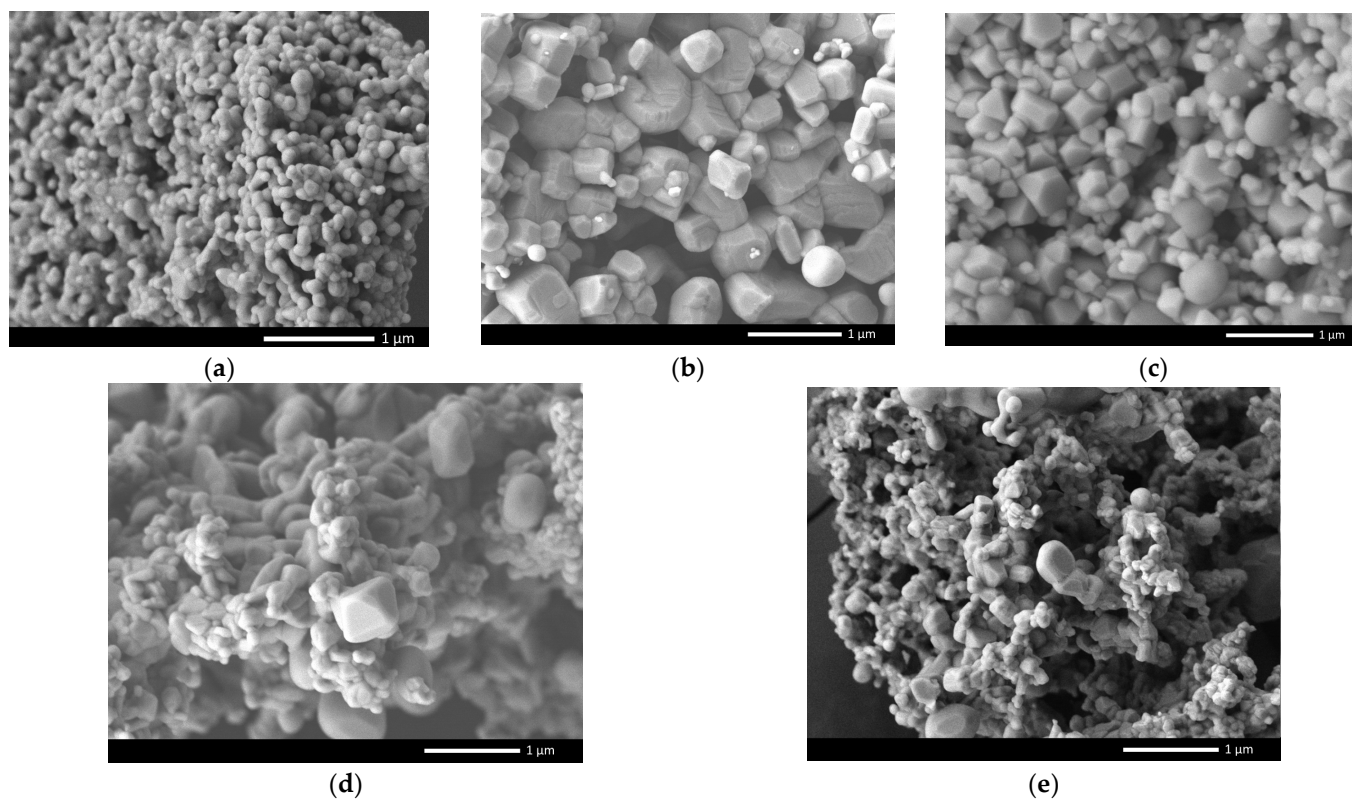


Figure 1. Data on the morphological features of the synthesized iron-containing nanocomposites: (a) Fe_2O_3 nanoparticles; (b) $\text{Fe}_2\text{O}_3@\text{GdFeO}_3$ nanoparticles; (c) $\text{Fe}_2\text{O}_3@\text{NdFeO}_3$ nanoparticles; (d) CeFeO_3 nanoparticles; (e) YFeO_3 nanoparticles.

An analysis of the morphological features of nanoparticles subjected to thermal annealing after mechanochemical grinding made it possible to establish the following. Firstly, thermal annealing of unmodified Fe_2O_3 nanoparticles leads to the formation of spherical structures, the size of which varies in the range of 90–100 nm, the size isotropy being more than 90%, and the deviation from the average size not exceeding 5–7 nm. In the case of doping with gadolinium, the shape of the grains undergoes significant changes, including the formation of rhomboid or cubic grains, the size of which reaches 300–400 nm, while the structure contains a small number of spherical grains, the size of which is from 50 to 200 nm. Such a change in the particle shape can be explained primarily by sintering processes, which are activated by the addition of low-melting gadolinium nitrate ($T_{\text{melting}} = 91^\circ\text{C}$). In this case, gadolinium contributes to the acceleration of the processes of fusion of iron-containing particles into larger agglomerates with their subsequent transformation from spherical to diamond-shaped or cubic shape.

A similar situation is observed in the case of thermal annealing of a milled sample of iron-containing nanoparticles with Nd_2O_3 , for which a change in the particle shape is also observed; however, unlike nanocomposites with gadolinium nitrate, the sizes of the obtained nanoparticles do not exceed 120–140 nm.

In the case of adding cerium and yttrium oxide, the shape of the resulting nanocomposites is dendritic, consisting of spherical or cubic particles, the average size of which varies from 50 to 100 nm.

3.2. X-ray Phase Analysis of the Studied Samples

Figure 2 shows diffractograms of the studied nanocomposites, presented in order to reflect their phase composition and characterization of structural parameters. Hematite (Fe_2O_3) nanoparticles synthesized by the chemical co-precipitation method used to obtain the initial iron-containing components of nanocomposites, annealed at a temperature of 800°C , were also selected as samples for comparison in order to determine the effectiveness of doping with rare earth elements on adsorption and degradation resistance.

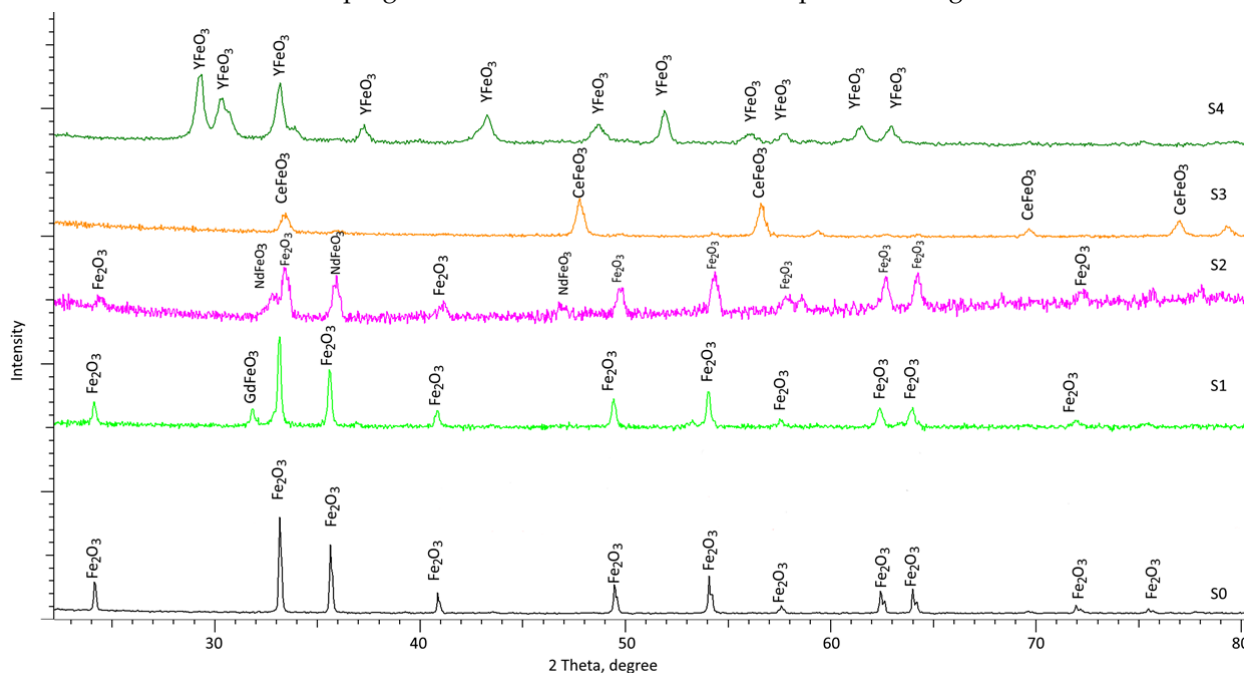


Figure 2. Characterization results of the phase composition of synthesized objects of study: S0— Fe_2O_3 nanoparticles; S1— Fe_2O_3 @ GdFeO_3 nanoparticles; S2— Fe_2O_3 @ NdFeO_3 nanoparticles; S3— CeFeO_3 nanoparticles; S4— YFeO_3 nanoparticles.

According to the presented data of X-ray phase analysis, it was found that the initial nanoparticles annealed at a temperature of 800°C can be characterized by a hematite (Fe_2O_3) phase with a rhombohedral type of crystal lattice, spatial syngony $R\text{-}3c(167)$. The crystal lattice parameters of the sample in the initial state were $a = 5.0335 \text{ \AA}$ and $c = 13.7434 \text{ \AA}$, which differs somewhat from the reference values for the Fe_2O_3 hematite phase (PDF-00-033-0664) ($a = 5.0356 \text{ \AA}$, $c = 13.4589 \text{ \AA}$). Such a small difference is associated primarily with the processes of obtaining nanoparticles, as well as subsequent thermal annealing of the samples, which is accompanied by the structural ordering of nanoparticles and their sintering into larger agglomerates.

When using mechanochemical grinding of chemically synthesized iron-containing nanoparticles with the addition of $\text{Gd}(\text{NO}_3)_3$, and subsequent thermal annealing at a temperature of 800°C , the phase composition of the resulting nanocomposite is a mixture of two phases: hematite Fe_2O_3 with a rhombohedral type of crystal lattice and with an orthorhombic GdFeO_3 phase. Additionally, the assessment of the weight contributions of these phases in the composition of nanocomposites, based on the assessment of the areas of reflections characteristic of these phases, showed that the dominant phase in the composition is the hematite phase (more than 94%), while the content of the GdFeO_3 phase is slightly more than 5%. Additionally, analyzing the changes in the crystal lattice parameters for the Fe_2O_3 phase ($a = 5.0423 \text{ \AA}$, $c = 13.7379 \text{ \AA}$), it can be concluded that the upward deviation is associated with the partial replacement of iron ions by gadolinium ions, which leads to an increase in the parameters due to the difference in ionic radii. In turn, the formation of the GdFeO_3 phase at a low content can be due to the effect of

high substitution followed by the $\text{Fe}_2\text{O}_3 \rightarrow \text{GdFeO}_3$ transformation and a change in the spatial syngony.

For samples of iron-containing nanocomposites, the addition of the Nd_2O_3 compound also leads to the formation of two-phase structures containing the dominant Fe_2O_3 hematite phase with parameters $a = 4.9892 \text{ \AA}$, $c = 13.6653 \text{ \AA}$, as well as the NdFeO_3 orthorhombic phase, characteristic of partial replacement of iron by neodymium. However, unlike samples containing gadolinium, in the case of samples with neodymium, the content of the impurity phase is at least 19%, which indicates that the processes of replacing iron with neodymium are more intense than for gadolinium.

In the case of using CeO_2 and Y_2O_3 during mechanochemical mixing with iron oxide and subsequent thermal annealing at 800°C , according to X-ray diffraction data, the structure of the resulting nanocomposites can be characterized by the orthorhombic CeFeO_3 and YFeO_3 phases characteristic of substitutional phases. Additionally, the presence of a hematite phase was not found in the composition of both nanocomposites. This behavior for these structures can be due to the fact that the addition of CeO_2 and Y_2O_3 oxides during mechanochemical grinding and subsequent thermal annealing leads to the formation of substitution phases due to the higher mobility of cerium and yttrium ions, whose oxides are in most cases used to stabilize ceramics during thermal sintering.

One of the important criteria in assessing the effect of doping nanostructures with various elements is the assessment of structural ordering (the degree of crystallinity), which reflects how much the formation of additional phases in the composition of nanocomposites affects ordering. The structural ordering degree was estimated by a comparative analysis of the obtained diffractograms and structural parameters of the crystal lattice, and Figure 3 shows the dependence of the change in this value on the composition of nanoparticles in comparison with unmodified annealed Fe_2O_3 nanoparticles.

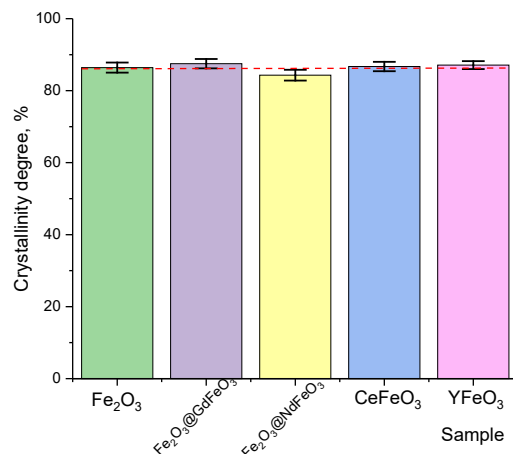


Figure 3. Assessment results of the structural ordering degree of the synthesized nanocomposites.

As can be seen from the data presented, thermal annealing of the studied nanocomposites subjected to mechanochemical grinding leads to the formation of well-structurally ordered nanoparticles, the structural ordering degree of which is more than 80%. In this case, variation in the components for doping does not lead to significant changes in the structural ordering degree, which can be explained by the formation of impurity phases in the structure of nanoparticles in the form of substitution solutions or the complete transformation of the Fe_2O_3 phase into the substitutional solid solution phase.

3.3. Mössbauer Spectrometry of the Studied Nanocomposites

Figure 4 shows the results of Mössbauer spectrometry of the studied samples of nanocomposites, presented in the form of Mössbauer spectra, and the results of the dependence of the distribution of magnetic fields. The general view of the presented Mössbauer

spectra for all nanocomposites under study is characterized by a set of Zeeman sextets, as well as small quadrupole doublets, which are characteristic of paramagnetic inclusions and regions of structural disorder. The presented values of hyperfine magnetic fields are also typical for the Fe_2O_3 structure with various degrees of its modification caused by the effects of the formation of substitution phases in the case of doped structures.

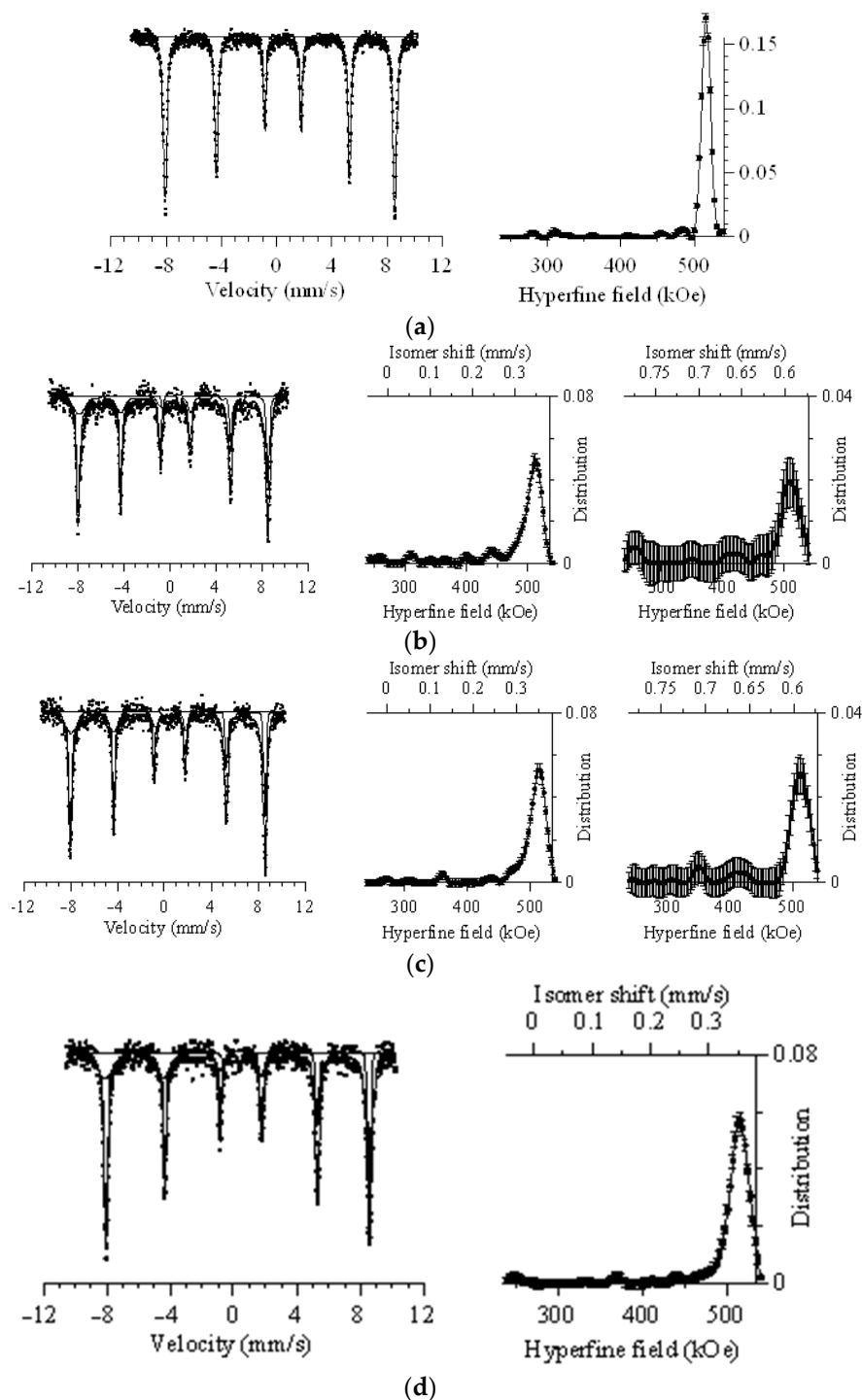


Figure 4. Cont.

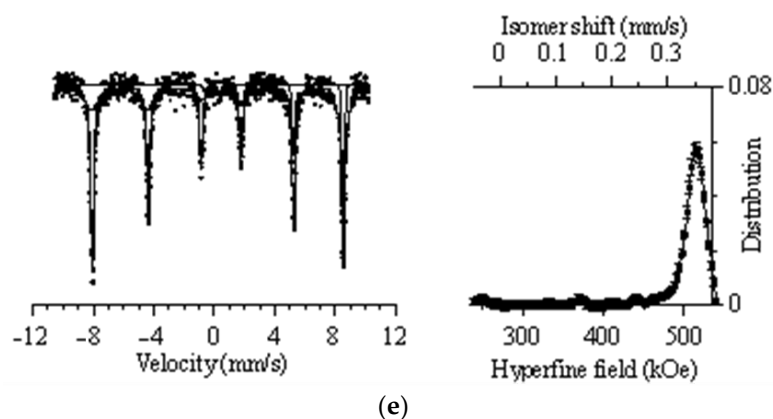


Figure 4. Mössbauer spectra of the studied nanocomposites: (a) Fe_2O_3 nanoparticles; (b) $\text{Fe}_2\text{O}_3@\text{GdFeO}_3$ nanoparticles; (c) $\text{Fe}_2\text{O}_3@\text{NdFeO}_3$ nanoparticles; (d) CeFeO_3 nanoparticles; (e) YFeO_3 nanoparticles.

According to the analysis of the obtained Mössbauer spectrum for Fe_2O_3 nanoparticles annealed at a temperature of 800°C , the following was established. The resulting spectrum can be characterized by a Zeeman sextet, the line ratio of which is characteristic of highly ordered iron oxide Fe_2O_3 , which is also confirmed by the hyperfine magnetic field, which is 515.64 ± 0.08 kOe, and the isomeric shift of 0.3782 ± 0.0015 . Additionally, when processing the obtained spectrum, the presence of characteristic partial spectra for quadrupole doublets was not found, which indicates the absence of magnetically disordered regions in the structure of nanoparticles.

For the modified nanoparticles, when deciphering the Mössbauer spectra, two characteristic Zeeman sextets were used, the choice of which is determined by the data on the phase composition, as well as a quadrupole doublet characterizing the magnetically disordered contributions. The general form of the spectra of modified particles has small differences in the intensity of the spectral lines compared to unmodified Fe_2O_3 nanoparticles, which is due to the effect of the substitution of iron ions by ions of rare earth elements in octo- and tetrahedral positions. For $\text{Fe}_2\text{O}_3@\text{GdFeO}_3$ nanoparticles, the presence of two partial spectra can be explained by the presence of Fe_2O_3 and GdFeO_3 phases. Moreover, the values of hyperfine magnetic fields for two spectra are 513.11 ± 1.00 kOe and 509.82 ± 2.90 kOe, which are typical for the ordered structure of hematite, as well as the modified iron oxide GdFeO_3 . The evaluation of the contributions of the partial spectra showed that the dominant contribution of more than 90% is the spectrum with characteristic field parameters of 513.11 ± 1.00 kOe, and the contribution of the second spectrum is no more than 8%, which is in good agreement with the data on the evaluation of the contributions of the Fe_2O_3 and GdFeO_3 phases from X-ray phase analysis. The contribution of the quadrupole doublet, according to estimates, was slightly more than 1.5%, which indicates only a small fraction of magnetically disordered or structurally disordered inclusions in the composition of nanoparticles.

A similar situation was also observed for $\text{Fe}_2\text{O}_3@\text{NdFeO}_3$ nanoparticles, whose spectra were also interpreted using two partial sextets describing the contributions of the Fe_2O_3 and NdFeO_3 phases. The characteristic values of hyperfine magnetic fields for two partial spectra were 512.72 ± 1.60 kOe and 511.46 ± 0.90 kOe, while the ratio of the intensities of the contributions of the two spectra was 78% and 19%, respectively, which is also in good agreement with the X-ray phase analysis data. Less than 3% was the contribution of the quadrupole doublet, which is characteristic of disordered inclusions. A slight increase in this contribution is also consistent with the data on the structural ordering degree, the value of which for $\text{Fe}_2\text{O}_3@\text{NdFeO}_3$ nanoparticles is somewhat less than for all other synthesized nanoparticles.

In the case of CeFeO_3 and YFeO_3 nanoparticles, a combination of a partial sextet and a quadrupole doublet was used for deciphering. According to the obtained data, the

values of hyperfine magnetic fields for two types of nanoparticles were 516.23 ± 0.70 kOe and 508.53 ± 0.40 kOe for CeFeO₃ and YFeO₃ nanoparticles, respectively. Additionally, the contribution of the quadrupole doublet was less than 0.7% and 1.1% for CeFeO₃ and YFeO₃ nanoparticles.

Thus, by analyzing the general data of processing the Mössbauer spectra of the synthesized nanoparticles, we can conclude that the main contribution to the formation of the parameters of the hyperfine magnetic field is made by the hematite structure with slightly distorted magnetic fields for the modified nanoparticles. This is primarily due to the effect of the replacement of iron ions by rare earth elements. Additionally, the comparison of the contributions of the partial spectra for Fe₂O₃@GdFeO₃ and Fe₂O₃@NdFeO₃ nanoparticles is in good agreement with the data on the evaluation of phase contributions from X-ray phase analysis.

3.4. Manganese Adsorption Experiments

The evaluation of the adsorbent properties of the synthesized nanocomposites was carried out during the following serial experiments. To determine the optimal concentration of nanocomposites in order to establish the efficiency of pollutant adsorption with the possibility of subsequent capture of nanoparticles and their extraction for reuse, concentrations from 0.01 g to 1 g of particles per a given volume of a model solution of 100 mL were chosen. Determination of the pollutant concentration in the model solution was determined within 5 h with a measurement interval of 30 min. The measurements were carried out at room temperature of the model solution, which was maintained using a shaker-incubator maintaining a temperature of 25 ± 1 °C. The results of the adsorption efficiency evaluation are shown in Figure 5.

The general view of the presented graphs has a pronounced dependence on the concentration of nanoparticles in the model solution, which is expressed both in an increase in the adsorption efficiency and in the time dependence of achieving the maximum decrease in the concentration of manganese. As can be seen from the analysis of the obtained data on the assessment of changes in the concentration of manganese as a result of adsorption, an increase in the mass of nanoparticles from 0.01 g to 0.25 g used as an adsorbent leads to an increase in the efficiency of manganese adsorption, expressed in a decrease in its concentration. Additionally, Fe₂O₃@GdFeO₃ and Fe₂O₃@NdFeO₃ nanoparticles exhibit the highest adsorption efficiency when using them; after 300 min, the manganese content in the composition of the model solution is no more than 10–15% for masses of 0.10–0.25 g. In this case, at the same masses of CeFeO₃ and YFeO₃ nanoparticles, the concentration of manganese in the model solution after 300 min of adsorption was no more than 20%.

In the case of an increase in the mass of nanoparticles above 0.25 g, no significant changes in the efficiency of manganese adsorption were observed; however, the time for which the maximum decrease in the concentration of manganese for Fe₂O₃@GdFeO₃ and Fe₂O₃@NdFeO₃ nanoparticles is reached was significantly less than when using small masses. This behavior of the change in efficiency may be due to the fact that with an increase in the mass of nanoparticles, the number of interacting particles in the adsorption reactions increases, as a result of which the overall process of reducing the concentration of manganese occurs more intensively, while when a certain threshold is reached, the reactions stop. The achievement of the adsorption threshold is evidenced by the data presented in Figure 5e,f, which show the results of estimating the change in the concentration of manganese at nanoparticle masses of 0.5 and 1.0 g. In this case, the achievement of the maximum decrease in the concentration of manganese in the model solution during its adsorption by Fe₂O₃@GdFeO₃ and Fe₂O₃@NdFeO₃ nanocomposites occurs in 210 and 180 min in the case of nanoparticle concentrations of 0.5 and 1.0 g, respectively.

An increase in the mass of nanoparticles affects the efficiency of unmodified Fe₂O₃ nanoparticles, for which an increase in mass leads to an increase in the purification efficiency from 15–20% to 60–70%. In this case, in contrast to modified nanoparticles for Fe₂O₃

nanoparticles, an increase in mass above 0.25 g also leads to an increase in the efficiency of purification of aqueous solutions.

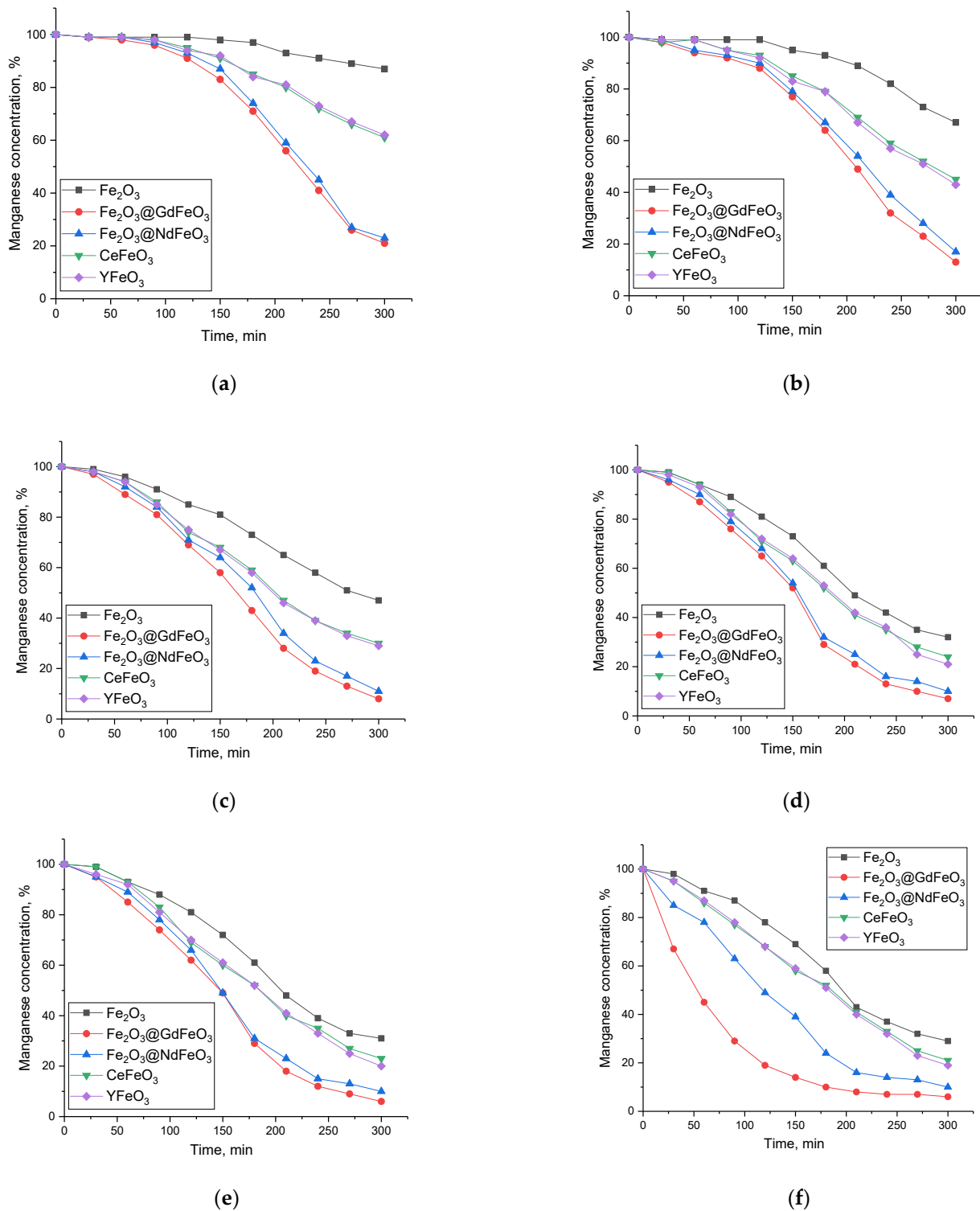


Figure 5. Evaluation results of the manganese concentration change in model solutions depending on time with different contents of the weight fraction of nanoparticles in the model solution: (a) 0.01 g; (b) 0.05 g; (c) 0.10 g; (d) 0.25 g; (e) 0.50 g; (f) 1.00 g.

The efficiency degree was calculated by comparing the values of the measured optical density of the solution depending on the adsorption time with the initial value. Figure 6 shows the assessment results of the adsorption efficiency with a variation in the mass of nanoparticles in a model solution. To calculate the adsorption efficiency, Formula (2) [20] was used:

$$R = \frac{C_0 - C_f}{C_0} \times 100\% \quad (2)$$

where C_0 and C_f are concentrations of manganese in the initial and final state.

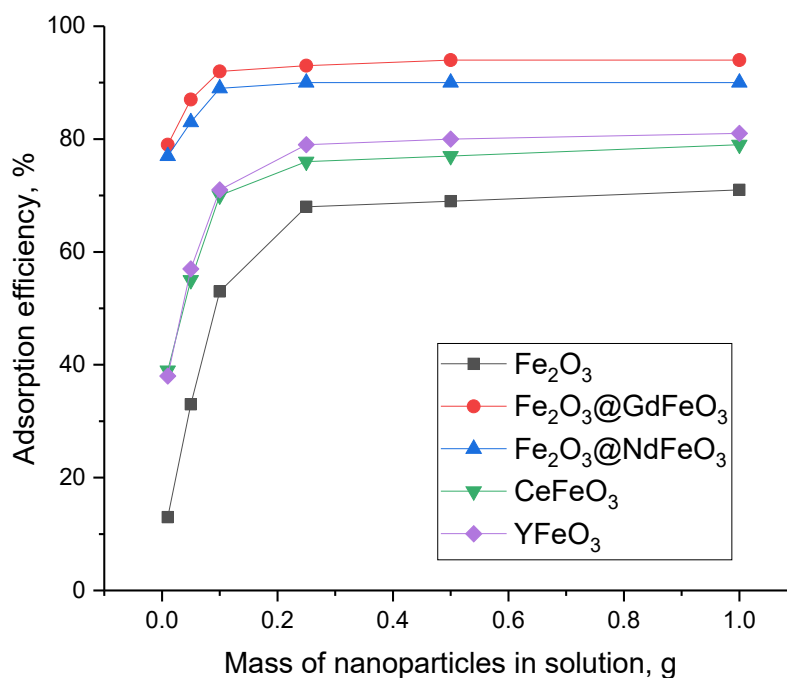


Figure 6. Results of changes in the manganese adsorption efficiency with variation in the mass of nanoparticles in a model solution.

As can be seen from the presented data, an increase in the mass of nanoparticles in aqueous solutions leads to an increase in the adsorption efficiency; however, these changes have a saturation limit, which is reached at a mass of 0.25 g. With a further increase in the mass of nanoparticles, an increase in efficiency is practically not observed; however, it should be noted that, in this case, a decrease in the required time is observed to achieve the maximum purification of aqueous media. Moreover, this effect is most pronounced for Fe₂O₃@GdFeO₃ and Fe₂O₃@NdFeO₃ nanoparticles (see data in Figure 5e–g).

In order to study the adsorption kinetics, two models of pseudo-first and pseudo-second order were used, the use of which makes it possible to evaluate the rate of manganese sorption in comparison with the sorption capacity and efficiency. The calculation formulas for these models were taken from [20]. The presented dependences of the kinetic curves of manganese adsorption reactions can be described using the Akaike information criterion (AIC) [20], which makes it possible to calculate the optimal time to reach the highest efficiency, as well as the rate constants of adsorption reactions.

Figure 7 shows the results of the assessment of the construction of kinetic curves of the adsorption reaction in order to determine the reaction rate constant as a function of time. The data are given for all studied nanoparticles depending on their concentration in model solutions. Figure 8 shows the results of evaluating pseudo-second-order kinetic curves.

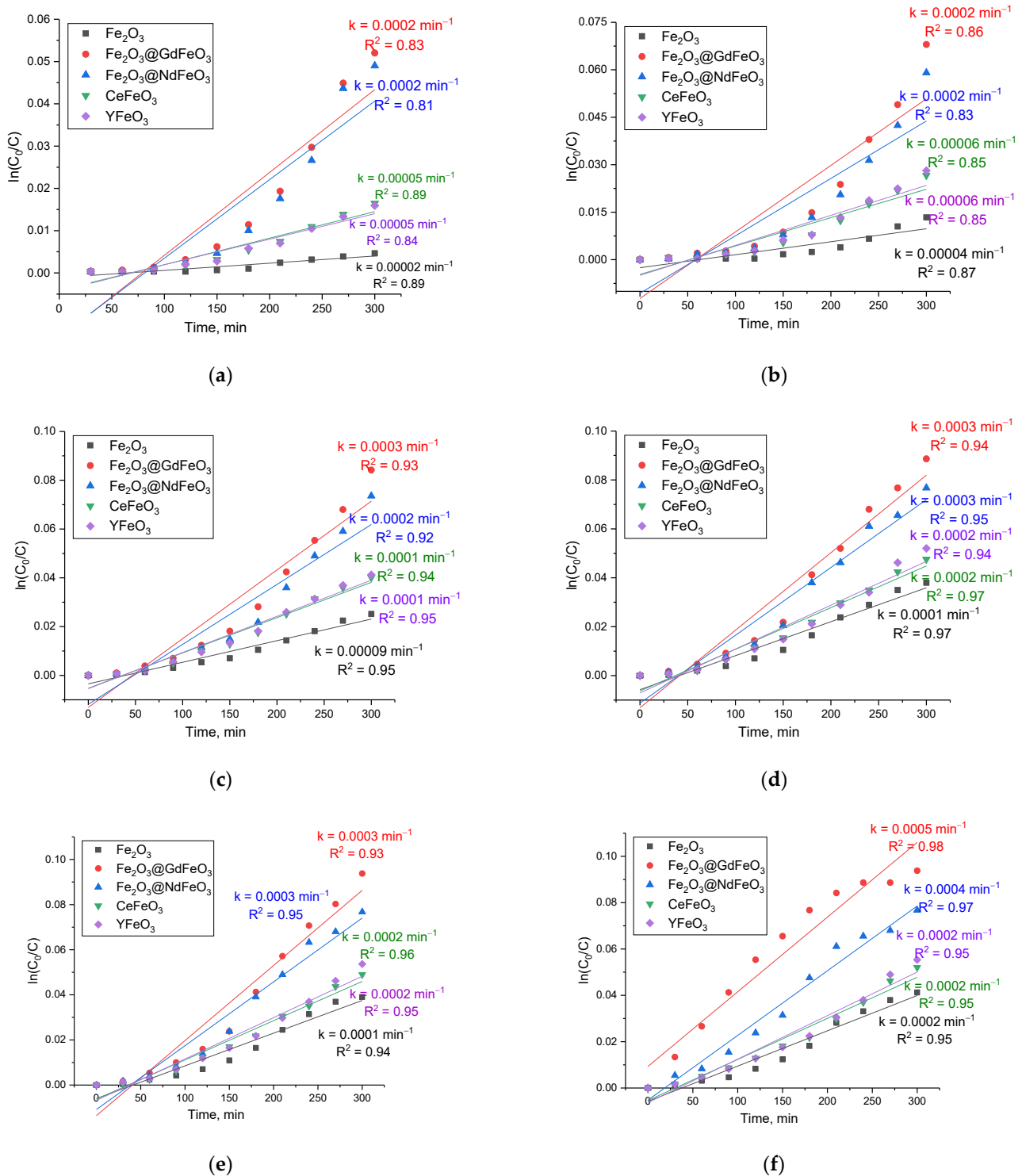


Figure 7. Results of the construction of adsorption reaction kinetic curves in order to determine the reaction rate constant for the studied nanoparticles with a variation in their mass in solution: (a) 0.01 g; (b) 0.05 g; (c) 0.10 g; (d) 0.25 g; (e) 0.50 g; (f) 1.00 g.

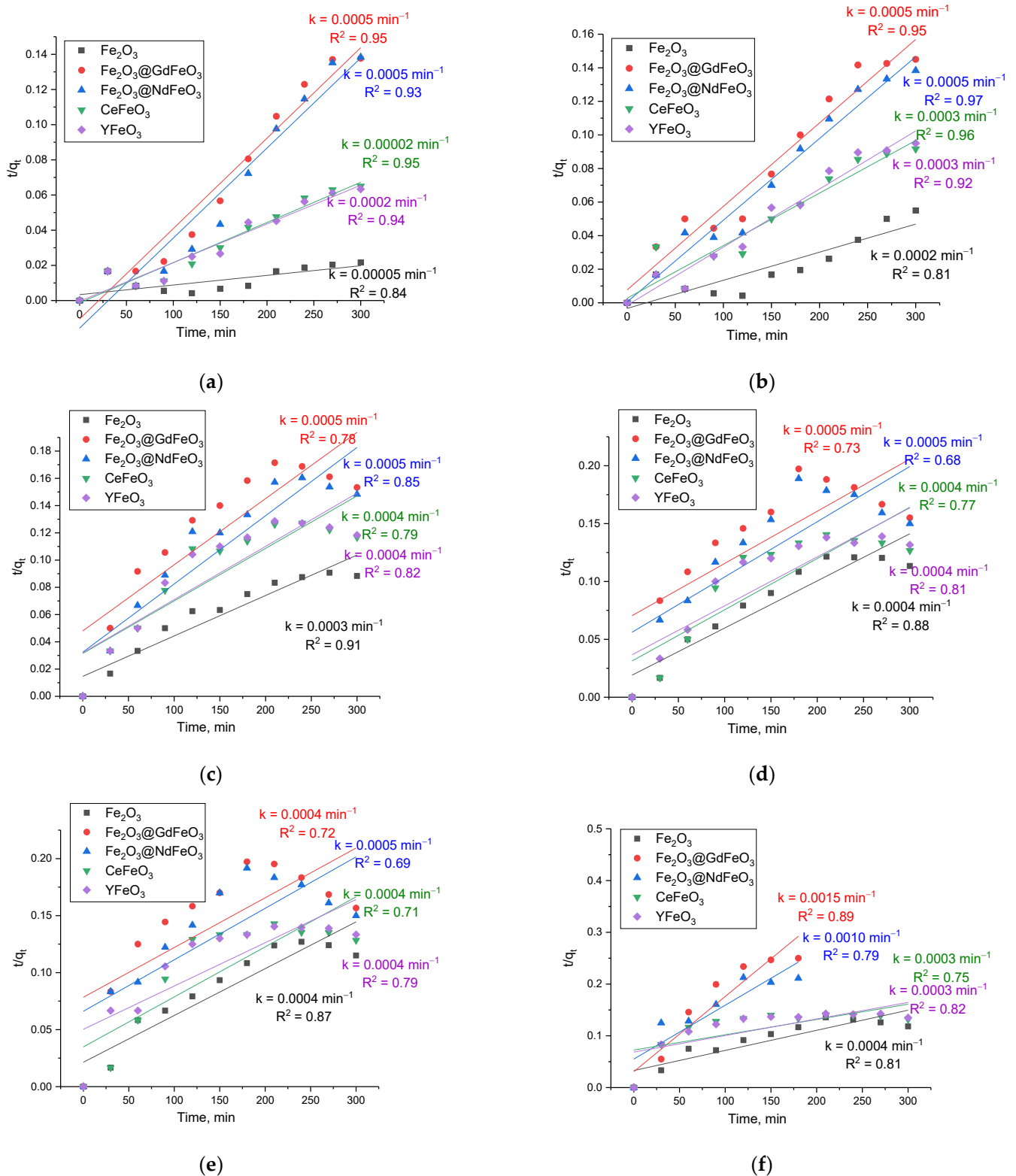


Figure 8. Results of constructing pseudo-second-order kinetic curves of the adsorption reaction to determine the rate constant of the reaction of the studied nanoparticles with a change in their mass in solution: (a) 0.01 g; (b) 0.05 g; (c) 0.10 g; (d) 0.25 g; (e) 0.50 g; (f) 1.00 g.

The very mechanism of manganese extraction from aqueous solutions can be explained by the cation exchange of manganese ions (Mn^{2+}) with the surface of nanocomposites. Additionally, the formation of binary phases of the $\text{Fe}_2\text{O}_3@\text{GdFeO}_3$, $\text{Fe}_2\text{O}_3@\text{NdFeO}_3$ type or phases characteristic of complex oxides of the CeFeO_3 , YFeO_3 type in the structure of nanocomposites leads to a change in the electronic structure, and, as a consequence, a change in the Van der Waals forces on the surface of the nanocomposites. Moreover, a change in the phase composition, as can be seen from these morphological features, leads to a change in the shape and size of nanoparticles, which affects the adsorbing surface and is quite developed in the case of modified nanocomposites (see data in Figure 1). In the case of using $\text{Fe}_2\text{O}_3@\text{GdFeO}_3$ and $\text{Fe}_2\text{O}_3@\text{NdFeO}_3$ nanocomposites, an increase in the adsorption efficiency can be due to the mechanisms of the transfer of Mn^{2+} ions from an aqueous solution to the surface of the nanocomposite as a result of the action of force fields, which are determined both by the fields of hematite and by substitution phases of the GdFeO_3 and NdFeO_3 types and are formed during synthesis. Additionally, in comparison with pure hematite (Fe_2O_3), for which the adsorption efficiency is rather low even at high adsorbent concentrations in an aqueous solution, the presence of GdFeO_3 and NdFeO_3 phases in the composition of nanocomposites has a significant effect on the adsorption efficiency. Therefore, it can be concluded that the modification of iron-containing nanoparticles plays a very important role in the efficiency of adsorption. Additionally, the obtained results of the influence of modification on the adsorption mechanisms are in good agreement with the work [21], according to which the functionalization of the surface of iron-containing nanoparticles significantly increases the efficiency of heavy metal sorption. Moreover, an increase in the efficiency of manganese adsorption by composites with rare earth elements is due to a more developed surface, as well as the presence of a cation exchange interaction, which was reported in [22,23].

As can be seen from the data presented, almost all observed changes in the kinetic curves can be described by a straight line. This indicates that the adsorption processes themselves can be described by reactions of the first order, on the basis of which the reaction rate constant was determined, the change of which is most pronounced with an increase in concentration from 0.1 to 0.25 g for modified nanoparticles, and for Fe_2O_3 nanoparticles from 0.25 to 1.0 g.

Table 1 presents the results of the estimated parameters of the kinetic models used to evaluate the obtained results of manganese adsorption using various nanocomposites.

By analyzing the obtained data of pseudo-first- and pseudo-second-order kinetic curves for the studied nanocomposites, we can draw the following conclusions. Firstly, the concentrations of nanoparticles of 0.1–0.25 g, for which the reaction rate varies from 1×10^4 to $5 \times 10^4 \text{ min}^{-1}$, depending on the type of nanocomposites, are the most effective for the adsorption of manganese from aqueous solutions. Additionally, of the two proposed models, according to the AIC values, the most suitable for describing the obtained kinetic curves is the use of the pseudo-first-order model, for which the AIC values at various adsorbent concentrations are the smallest in comparison with similar data for the pseudo-second-order model. Moreover, the use of the pseudo-second-order model showed a significant deterioration in the description of the curves since the adsorption process itself at high concentrations proceeds much faster for modified nanocomposites and reaches the saturation effect after 180–210 min of adsorption.

Table 1. Estimated parameters of pseudo-first- and pseudo-second-order kinetic models for manganese adsorption using various nanocomposites.

Sample	Concentration of Adsorbent, g	Pseudo-First-Order Parameters				Pseudo-Second-Order Parameters			
		K (min ⁻¹)	q _e (mg/g)	R ²	AIC Values	K (g mg ⁻¹ min ⁻¹)	q _e (mg/g)	R ²	AIC Values
Fe ₂ O ₃	0.01	2 × 10 ⁵	0.652	0.89	45.32	5 × 10 ⁵	0.648	0.84	66.43
	0.05	4 × 10 ⁵	0.331	0.87	48.53	2 × 10 ⁴	0.325	0.81	77.35
	0.10	9 × 10 ⁵	0.265	0.95	32.35	3 × 10 ⁴	0.297	0.91	57.54
	0.25	1 × 10 ⁴	0.136	0.97	28.43	4 × 10 ⁴	0.147	0.88	67.85
	0.5	1 × 10 ⁴	0.069	0.94	33.64	4 × 10 ⁴	0.073	0.87	65.64
	1.0	2 × 10 ⁴	0.035	0.95	32.43	4 × 10 ⁴	0.039	0.81	69.32
Fe ₂ O ₃ @GdFeO ₃	0.01	2 × 10 ⁴	3.952	0.83	49.34	5 × 10 ⁴	3.959	0.95	54.65
	0.05	2 × 10 ⁴	0.871	0.86	48.53	5 × 10 ⁴	0.885	0.95	52.54
	0.10	3 × 10 ⁴	0.461	0.93	43.23	5 × 10 ⁴	0.463	0.78	79.56
	0.25	3 × 10 ⁴	0.186	0.94	39.64	5 × 10 ⁴	0.185	0.73	89.63
	0.5	3 × 10 ⁴	0.094	0.93	34.56	4 × 10 ⁴	0.091	0.72	91.26
	1.0	5 × 10 ⁴	0.047	0.98	27.54	1.5 × 10 ³	0.102	0.89	38.43
Fe ₂ O ₃ @NdFeO ₃	0.01	2 × 10 ⁴	3.851	0.81	59.43	5 × 10 ⁴	3.845	0.93	64.35
	0.05	2 × 10 ⁴	0.832	0.86	47.85	5 × 10 ⁴	0.846	0.97	62.23
	0.10	2 × 10 ⁴	0.445	0.92	39.54	5 × 10 ⁴	0.441	0.85	74.64
	0.25	3 × 10 ⁴	0.181	0.95	32.24	5 × 10 ⁴	0.193	0.68	89.35
	0.5	3 × 10 ⁴	0.092	0.95	31.36	5 × 10 ⁴	0.095	0.69	91.23
	1.0	4 × 10 ⁴	0.045	0.97	25.65	1 × 10 ³	0.093	0.79	59.74
CeFeO ₃	0.01	5 × 10 ⁵	1.952	0.89	44.95	2 × 10 ⁴	1.945	0.95	63.42
	0.05	6 × 10 ⁵	0.552	0.85	47.53	3 × 10 ⁴	0.547	0.96	62.34
	0.10	1 × 10 ⁴	0.353	0.96	32.23	4 × 10 ⁴	0.357	0.79	72.42
	0.25	2 × 10 ⁴	0.152	0.95	33.24	4 × 10 ⁴	0.157	0.77	79.45
	0.5	2 × 10 ⁴	0.077	0.95	34.22	4 × 10 ⁴	0.074	0.71	82.44
	1.0	3 × 10 ⁴	0.039	0.96	29.45	3 × 10 ⁴	0.034	0.75	73.46
YFeO ₃	0.01	5 × 10 ⁵	1.902	0.84	53.56	2 × 10 ⁴	1.896	0.94	62.53
	0.05	6 × 10 ⁵	0.573	0.85	51.23	3 × 10 ⁴	0.569	0.92	62.24
	0.10	1 × 10 ⁴	0.355	0.95	36.54	4 × 10 ⁴	0.363	0.82	69.53
	0.25	2 × 10 ⁴	0.158	0.94	35.43	4 × 10 ⁴	0.149	0.81	78.45
	0.5	2 × 10 ⁴	0.082	0.96	31.45	4 × 10 ⁴	0.089	0.79	79.62
	1.0	2 × 10 ⁴	0.041	0.95	32.34	3 × 10 ⁴	0.039	0.82	73.22

3.5. Results of Evaluation of Adsorption Efficiency in Cyclic Tests

An important factor in the applicability of nanocomposites as adsorbents or catalysts is their resistance to prolonged exposure to aqueous media, which characterizes the stability of their crystal structure to degradation, as well as the possibility of reuse as adsorbents. Therefore, to test the applicability of the synthesized nanocomposites for the possibility of reuse and maintain stable indicators of the efficiency of pollutant adsorption, a series of experiments were carried out, the results of which are presented in Figure 9. Cycling was performed for all the studied samples of nanoparticles in model solutions at a concentration of 0.25 g, which showed the highest efficiency since it was shown above that an increase in the mass of nanoparticles above 0.25 g does not lead to a significant increase in the adsorption efficiency.

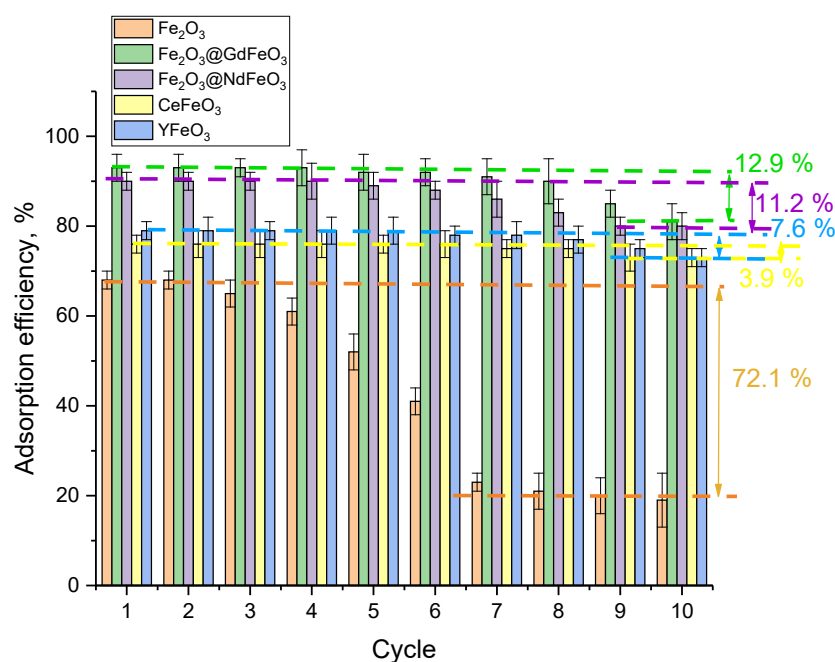


Figure 9. Evaluation results of changes in adsorption efficiency as a result of cyclic tests with repeated use of nanoparticles.

As can be seen from the presented data, Fe₂O₃ nanoparticles undergo the greatest decrease in adsorption efficiency during cyclic tests, for which a drop in efficiency is observed already after three cycles, and the maximum deterioration after 10 test cycles is more than 70%. Such a deterioration in the adsorbing capacity of Fe₂O₃ nanoparticles during cyclic tests can be explained by amorphization or destruction of nanoparticles during a long stay in the model solution, as well as during the interaction of the nanoparticle surface with both the model solution and heavy metal ions extracted from it. For modified nanoparticles, the highest resistance to long-term cyclic tests, despite the lower adsorption efficiency, was shown by CeFeO₃ and YFeO₃ nanoparticles, for which a decrease in efficiency is observed only after 6–7 cycles, and the decrease was 7.6% and 3.9%, respectively. This is somewhat lower than for Fe₂O₃@GdFeO₃ and Fe₂O₃@NdFeO₃ nanoparticles, for which a decrease in efficiency is observed after 5 cycles, and the decrease after 10 cycles was more than 10%. However, by analyzing the obtained data, we can conclude that nanoparticles modified with Fe₂O₃@GdFeO₃ and Fe₂O₃@NdFeO₃ are highly promising for the treatment of aqueous media due to high efficiency rates (more than 90%), as well as the stability of maintaining the cleaning efficiency during cyclic tests (at least five cycles). It should be noted that at lower adsorption efficiency (no more than 80%) of CeFeO₃ and YFeO₃, nanoparticles are more resistant to long-term tests, which can be used for frequent purification of aqueous media at low concentrations of heavy metals.

3.6. Results of Evaluation of Resistance to Degradation during Cyclic Tests

The assessment of resistance to degradation during long-term exposure to aqueous solutions was carried out by placing nanoparticles in a model medium for a period of 10 days, after which the morphological features of the obtained composites were visualized, and changes in their structural parameters were evaluated using the X-ray diffraction method. The results of these changes in morphological features are shown in Figure 10. Figure 11 shows the diffractograms of the test samples after 10 days of corrosion testing. During analysis of the data obtained, it was found that there was no new diffraction reflections characteristic of impurity inclusions formed as a result of degradation. The main changes are associated with a change in the shape of reflections and their intensity, which indicates a change in the degree of structural ordering.

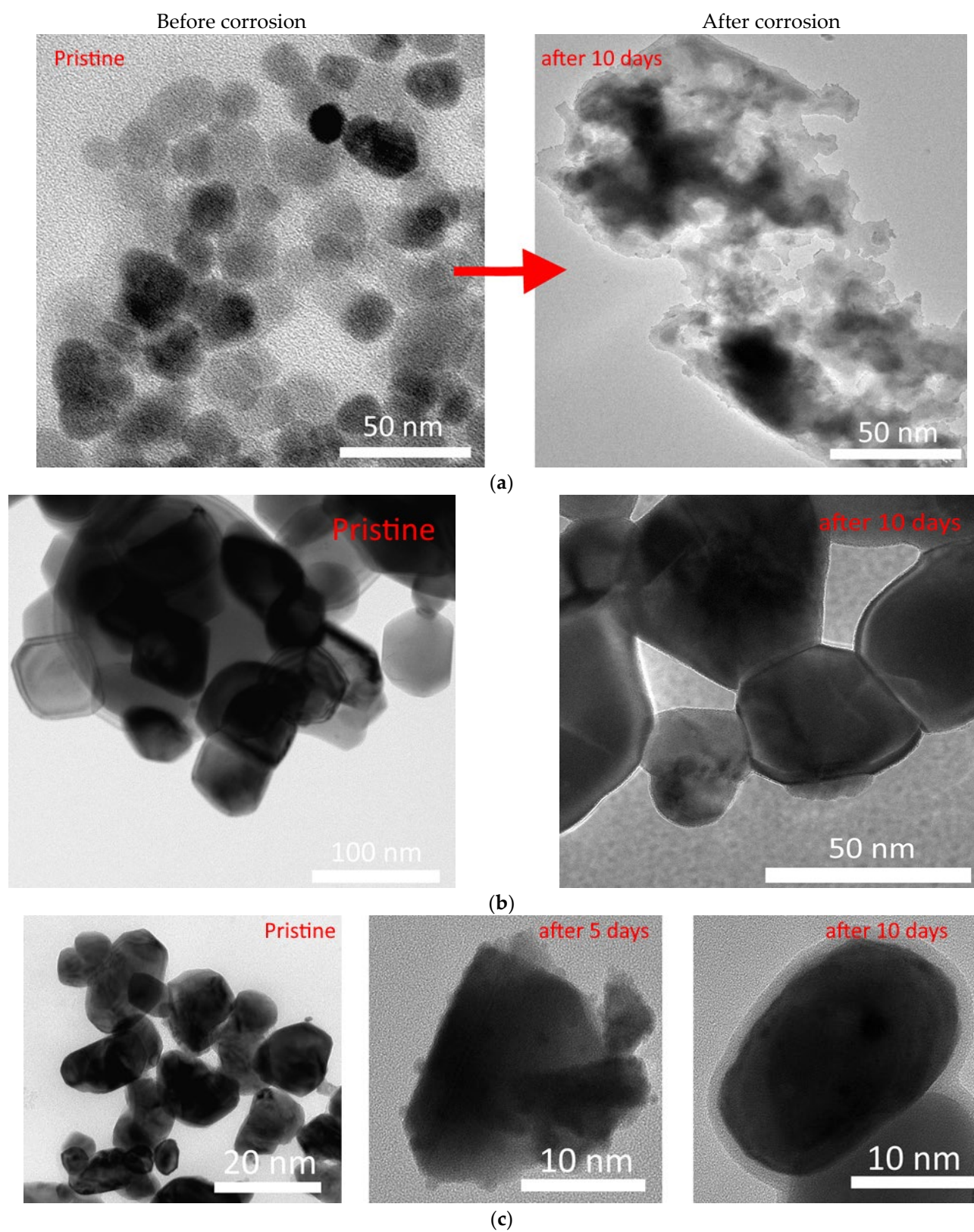


Figure 10. Cont.

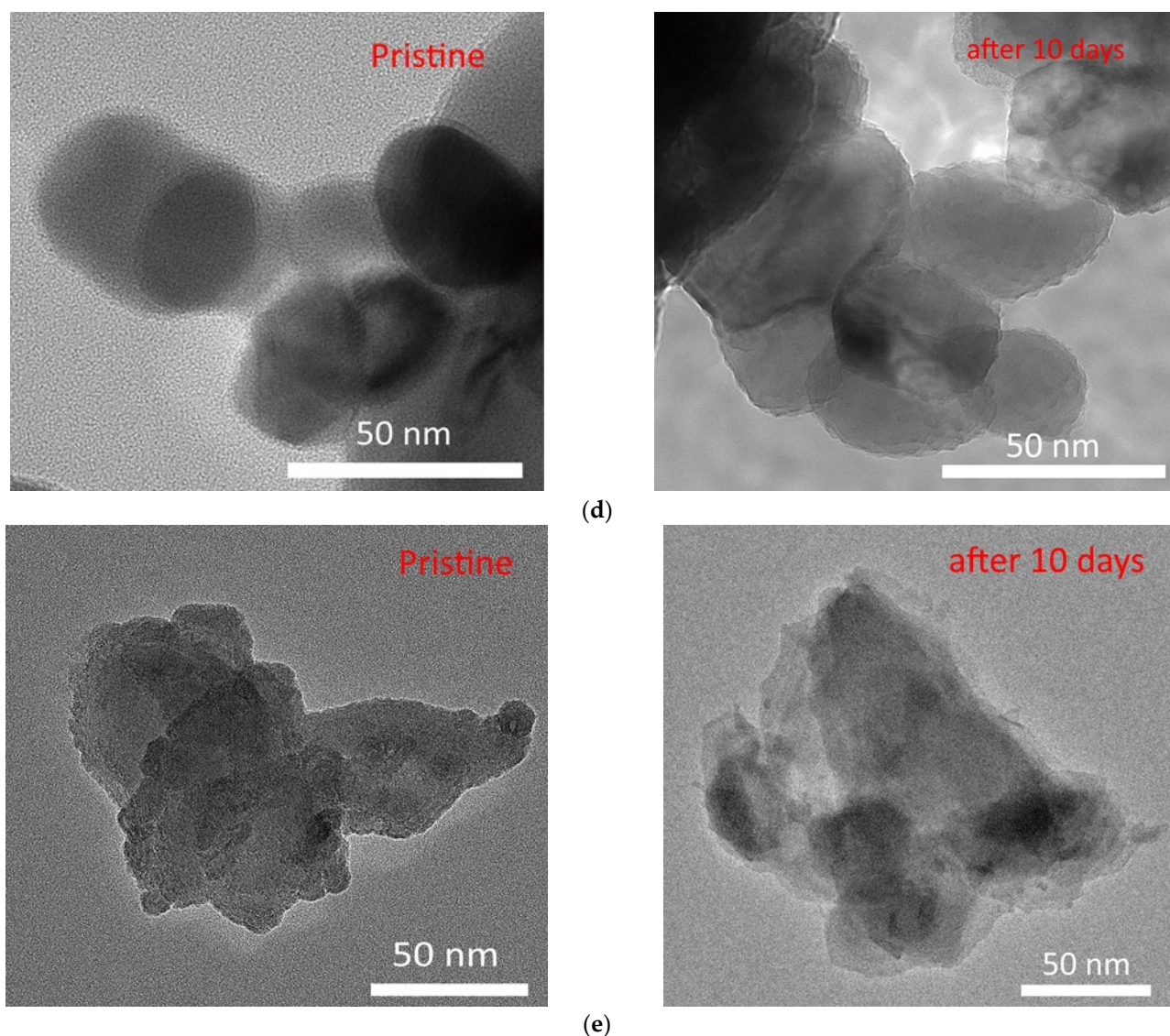


Figure 10. TEM images of the dynamics of changes in the morphological features of the studied nanocomposites before and after corrosion in a model solution: (a) Fe_2O_3 nanoparticles; (b) $\text{Fe}_2\text{O}_3@\text{GdFeO}_3$ nanoparticles; (c) $\text{Fe}_2\text{O}_3@\text{NdFeO}_3$ nanoparticles; (d) CeFeO_3 nanoparticles; (e) YFeO_3 nanoparticles CeFeO_3 .

As can be seen from the presented data on the morphological features of the studied nanocomposites before and after corrosion tests in a model solution, the main changes are associated with the partial destruction of the surface of nanoparticles and the formation of various growths in the form of spherical or feather-like inclusions, as well as the formation of films, which were observed in the case of $\text{Fe}_2\text{O}_3@\text{NdFeO}_3$ nanoparticles.

In the case of annealed unmodified hematite nanoparticles, being in a model solution, degradation processes proceed through partial destruction and loss of shape, followed by transformation into amorphous particles. In the case of modified nanocomposites, the processes of corrosion and subsequent degradation are less pronounced than in the case of the original Fe_2O_3 nanoparticles, which indicates an increased resistance of the modified nanocomposites to degradation during prolonged exposure to aqueous media. This fact allows for concluding that the addition of rare-earth elements to iron-containing nanocomposites leads to an increase in their stability, as well as the preservation of the particle shape, which makes it possible to use them for a longer time than in the case of conventional unmodified Fe_2O_3 nanoparticles, which have a low resistance to destruction.

It should also be noted that the main morphological changes for modified nanoparticles during corrosion tests occur according to the classical mechanisms of surface layer oxidation, followed by the formation of oxide films or inclusions in the form of hemispherical or spherical outgrowths. However, in the case of YFeO_3 nanoparticles, as well as in the case of initial Fe_2O_3 nanoparticles, degradation is accompanied by a partial loss of particle shape due to its amorphization, although less pronounced than in the case of Fe_2O_3 nanoparticles. Moreover, by analyzing the obtained data, we can conclude that $\text{Fe}_2\text{O}_3@\text{GdFeO}_3$ nanoparticles have the highest resistance to degradation as a result of corrosion tests, for which changes in morphological features were practically not observed, which is also confirmed by the results of changes in the structural ordering degree, the comparative data of which are presented in Figure 12.

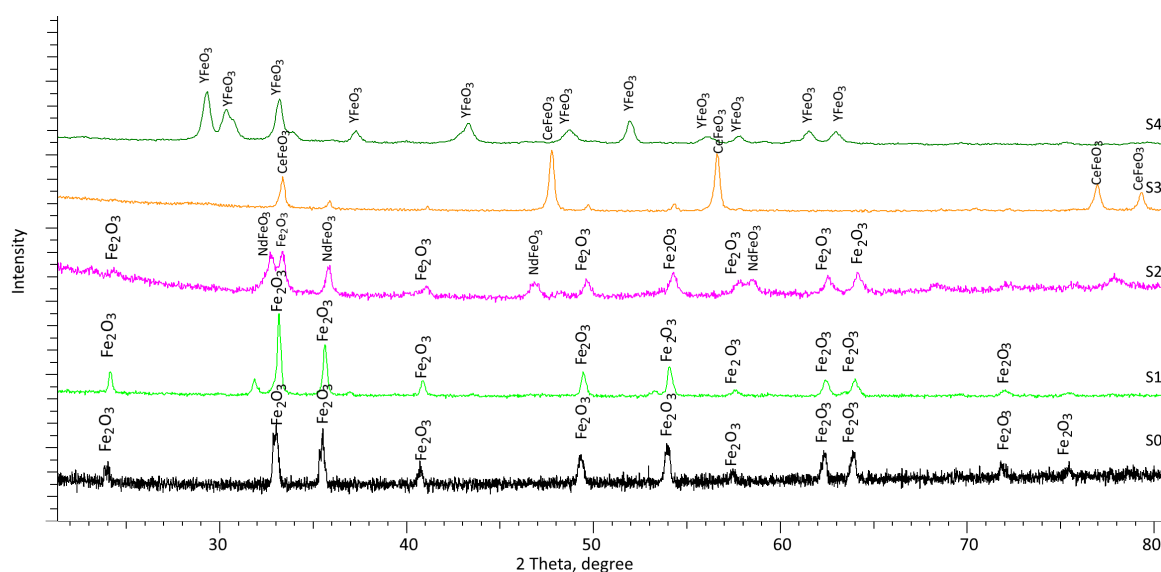


Figure 11. Diffractograms of samples after 10 days of corrosion testing.

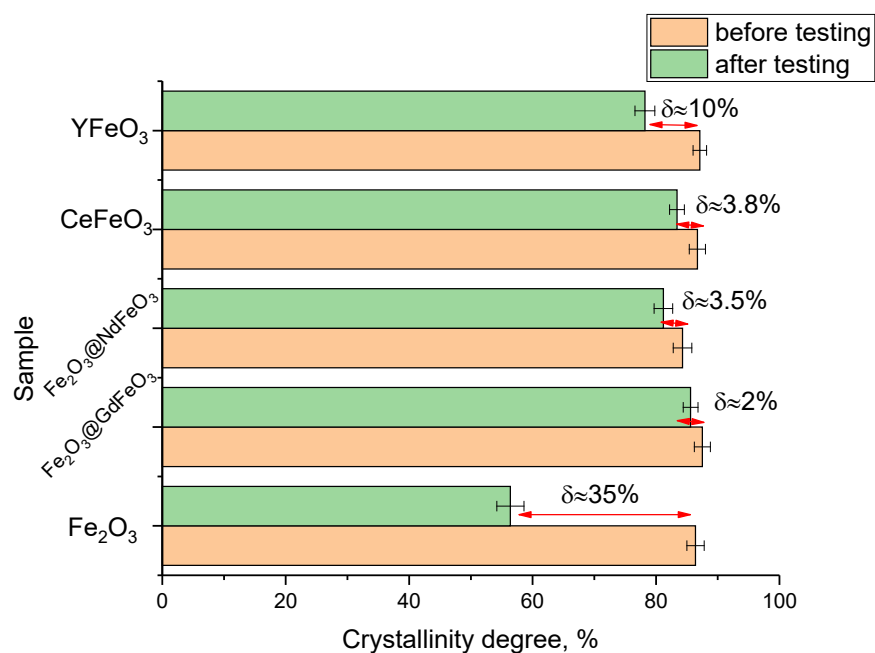


Figure 12. Results of the change in the structural ordering degree of the studied samples after corrosion tests (the data are given in comparison with the values in the initial state).

As can be seen from the presented data, the greatest changes in the structural ordering degree are observed for unmodified nanocomposites, the decrease for which is approximately 35% of the initial value. Moreover, a change of more than 10% is observed for samples of YFeO_3 nanoparticles, which, as can be seen from the data of morphological studies of transmission electron microscopy, are most susceptible to destruction in a model solution than other modified nanocomposites. In the case of $\text{Fe}_2\text{O}_3@\text{GdFeO}_3$, $\text{Fe}_2\text{O}_3@\text{NdFeO}_3$, and CeFeO_3 nanoparticles, the decrease in the degree of structural ordering is no more than 2–4% after 10 days of testing, which indicates a high resistance to degradation and corrosion during long-term exposure to the model solution. It is also worth noting that the modification of iron-containing nanoparticles leads to a 3- to 10-fold increase in resistance to degradation during corrosion in comparison with unmodified Fe_2O_3 nanoparticles.

3.7. Comparative Analysis of the Efficiency of Nanocomposites for Purification of Aqueous Media

The use of iron-containing nanocomposites obtained by mechanochemical mixing of iron oxide with compounds of rare earth elements and subsequent thermal annealing at a temperature of 800 °C as adsorbents for aqueous media purification has shown the high efficiency and promise of using these nanocomposites. Table 2 presents comparative data on the adsorption efficiency of the obtained nanocomposites.

Table 2. Comparative analysis results.

Parameter	Type of Nanocomposite				
	Fe_2O_3	$\text{Fe}_2\text{O}_3@\text{GdFeO}_3$	$\text{Fe}_2\text{O}_3@\text{NdFeO}_3$	CeFeO_3	YFeO_3
Adsorbent mass at which the maximum efficiency of manganese removal is achieved, g	1.0		0.25		0.5
Maximum manganese removal efficiency, %	69–71	93–94	89–90	77–80	79–81
Equilibrium time, min	270–300 min	270 min (at a concentration of 0.25 g) 180 min (at a concentration of 1.0 g)	270 min (at a concentration of 0.25 g) 210 min (at a concentration of 1.0 g)	270 min	270 min
Reaction rate constant, min^{-1}	0.00002–0.0002	0.0002–0.0005	0.0002–0.0004	0.00005–0.0002	0.00005–0.0002
Resistance to degradation during operation	Degrade by partial destruction after 10 days	Resistant to degradation after 10 days of testing	An oxide protective film is formed on the surface of nanocomposites	Covered with small growths	Partially amorphized after 10 days of testing
Number of recycles while maintaining maximum efficiency	After three cycles, adsorption efficiency drops sharply	After five consecutive cycles, there is a decrease in efficiency. After 10 cycles, a 10% decrease in efficiency.		After 6–7 cycles decrease in efficiency. The decrease in efficiency after 10 cycles is no more than 7–8%.	

As can be seen from the presented comparative table, the most effective are $\text{Fe}_2\text{O}_3@\text{GdFeO}_3$ and $\text{Fe}_2\text{O}_3@\text{NdFeO}_3$ nanocomposites, which have both high adsorption efficiency in shorter times and the possibility of stable use during successive cyclic or repeated tests. Additionally, in contrast to conventional hematite (Fe_2O_3), high adsorption efficiency is achieved with significantly lower masses of adsorbent from nanoparticles, which makes it possible to reduce its consumption in industrial use. It is also worth noting that the proposed technology for producing nanocomposites by mechanochemical mixing and heat treatment of Fe_2O_3 nanoparticles with rare earth compounds can significantly simplify the technological process for manufacturing such highly efficient adsorbents.

As is known, the key requirements for catalysts and adsorbents for the purification of aqueous media are a number of special requirements, including their physical properties, non-toxicity, and biocompatibility, as well as the efficiency of adsorption or photochemical decomposition. These requirements, as well as an assessment of the applicability of various types of nanoparticles in the purification of aqueous media, were formulated in detail in a number of reviews [24–26]. Therefore, one of the key requirements for nanoparticles in the case of their use as adsorbents or catalysts, in addition to their stability and adsorption efficiency, is their non-toxicity and decomposition into harmless components in case of degradation. In the case of the studied objects, it was previously shown in [27,28] that the resulting nanocomposites modified with rare earth elements gadolinium and neodymium are well biocompatible and do not have toxicity. Thus, the use of these modified nanoparticles as adsorbents will make it possible to eliminate the negative impact on aquatic environments and living organisms during use, and high stability indicators will allow these nanocomposites to be used for a sufficiently long time.

For comparison, the diagram (see Figure 13) presents comparative data on the efficiency of manganese adsorption using similar catalysts known from a number of literature data [29–33].

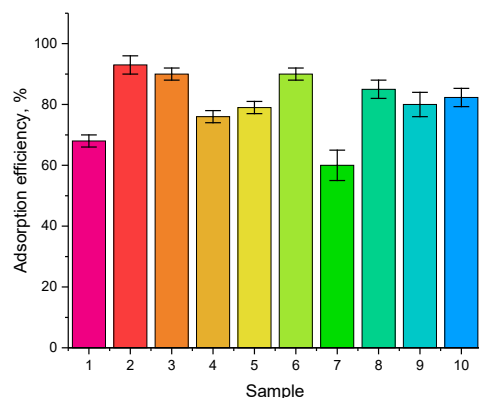


Figure 13. Comparative diagram of the adsorption efficiency of various types of nanocomposites: (1) Fe_2O_3 [this work]; (2) $\text{Fe}_2\text{O}_3@\text{GdFeO}_3$ [this work]; (3) $\text{Fe}_2\text{O}_3@\text{NdFeO}_3$ [this work]; (4) CeFeO_3 [this work]; (5) YFeO_3 [this work]; (6) $\text{Fe}_3\text{O}_4@\text{LDH}@\text{MnO}_2$ composite [29]; (7) Magnetite nanoparticles [30]; (8) $\text{Co}_x\text{Mn}_{1-x}\text{Fe}_2\text{O}_4$ nanocomposite [31]; (9) MgFe_2O_4 nanoparticles [32]; (10) $\text{FeNi}_3/\text{TiO}_2$ nanocomposite [33].

As can be seen from the presented data of the comparative diagram, the obtained $\text{Fe}_2\text{O}_3@\text{GdFeO}_3$ and $\text{Fe}_2\text{O}_3@\text{NdFeO}_3$ nanocomposites have a higher efficiency in comparison with other types of magnetic nanoparticles. Additionally, in the case of comparing the stability of the purification efficiency with the results of [29], $\text{Fe}_2\text{O}_3@\text{GdFeO}_3$ and $\text{Fe}_2\text{O}_3@\text{NdFeO}_3$ nanocomposites have a higher resistance to degradation during cyclic tests and the preservation of purification stability for five cycles. Moreover, when using $\text{Fe}_3\text{O}_4@\text{LDH}@\text{MnO}_2$ composite in cyclic tests, a decrease in adsorption efficiency was observed.

It should also be noted that, in most cases, the use of iron-containing nanoparticles or composites based on them as catalysts or adsorbents is due to their magnetic properties, which make it possible to extract particles after adsorption without mass loss and with the possibility of their reuse. All this plays an important role in assessing the prospects and economic feasibility of the application, as well as in calculating the cost of catalysts. In turn, the proposed technology for creating iron-containing composites modified with rare earth elements using simple technological operations, including mechanochemical grinding and thermal annealing, has a lower cost of manufacturing catalysts than using various types of chemical modification of nanoparticles using many different operations and expensive reagents.

3.8. Estimation of the Cost of Synthesized Nanocomposites

The cost estimate for the production of nanocomposites consists of the cost of purchasing chemical reagents, the time spent on manufacturing, taking into account grinding and subsequent thermal annealing, as well as the depreciation of equipment for synthesis and subsequent characterization of the obtained samples in order to establish the repeatability of the results. The pricing of the chemicals used for the synthesis was based on data provided by the official manufacturer and distributor Sigma Aldrich. Additionally, in the case of remote areas from the supplier, as a rule, it is also necessary to take into account the costs associated with transportation, which in most cases amount to 10–15% of the cost of goods from the manufacturer. Table 3 presents the cost of chemical reagents used for the manufacture of nanocomposites.

Table 3. Data on the cost of chemical reagents used for the production of nanocomposites.

Reagent Name	CAS No.	Pack Size, kg	Price, EUR
FeCl ₃ ·6H ₂ O	10025-77-1	1	195.00
Na ₂ SO ₃	7757-83-7	0.25	31.30
Gd(NO ₃) ₃	19598-90-4	0.01	139.00
Nd ₂ O ₃	1313-97-9	0.025	24.90
CeO ₂	1306-38-3	0.10	75.90
Y ₂ O ₃	1314-36-9	0.25	386.00

Thus, the cost of manufacturing 0.1 kg of the main component of iron oxide (Fe₂O₃), taking into account the cost of purchasing chemical reagents, as well as the depreciation of equipment and energy costs, is approximately EUR 30–40. The cost analysis took into account the cost of production, which was estimated at 30% of the total cost of the received product and included the cost of energy consumption and the use of equipment. For modified nanocomposites, the cost of 0.1 kg varies from EUR 50 to 150, where the main increase in the cost is associated with the price of the dopant, which, in the case of using the Gd(NO₃)₃ and Y₂O₃ components, is quite high, EUR 139 and EUR 386, respectively. However, even taking into account the high cost of rare earth components and the possibility of reusing these nanocomposites for purification (more than five consecutive cycles), the proposed nanocomposites are much cheaper than traditional catalysts based on noble metals such as palladium, gold, or silver. Additionally, it is important to note that the magnetic properties of the proposed nanocomposites allow them to be extracted from aqueous media without any significant losses, and the low toxicity and decomposability in water into harmless components makes it possible not to be afraid of contamination of water sources by nanocomposites during their use.

4. Conclusions

This paper presents the results of studies on the prospects of using mechanochemical synthesis to obtain iron-containing nanocomposites doped with rare earth elements in

order to increase the efficiency of heavy metal adsorption from aqueous media. According to the obtained data on morphological features, it was found that the addition of rare earth elements leads to a change in the shape of particles, as well as their enlargement, followed by the formation of agglomerate dendrite-like structures. According to the obtained test data for corrosion resistance, it was found that the modification of Fe_2O_3 nanoparticles with rare earth elements leads to an increase in the resistance to degradation and amorphization as a result of corrosion during prolonged exposure to an aqueous medium. Such increased stability can be explained by a change in the phase composition of iron-containing nanocomposites due to the formation of substitution phases in the form of impurity inclusions or a complete phase transformation of the $\text{Fe}_2\text{O}_3 \rightarrow \text{AFeO}_3$ ($\text{A} = \text{Ce}, \text{Y}$) type. During analysis of manganese adsorption data, it was found that nanoparticles modified with $\text{Fe}_2\text{O}_3@\text{GdFeO}_3$ and $\text{Fe}_2\text{O}_3@\text{NdFeO}_3$ are highly promising for the treatment of aqueous media due to high efficiency rates (more than 90%), as well as the stability of maintaining the cleaning efficiency during cyclic tests (at least five cycles). Additionally, it should be noted that with lower adsorption efficiency (no more than 80%) of CeFeO_3 and YFeO_3 , nanoparticles are more resistant to long-term tests, which can be used for frequent purification of aqueous media at low concentrations of heavy metals. Comparative analysis of the obtained results with the data of other works showed the high promise of the proposed nanostructures as adsorbents for the purification of aqueous media, which have a fairly low cost and ease of reproduction in any quantities.

Author Contributions: Conceptualization, K.K.K., A.L.K., K.B.E., I.E.K. and M.V.Z.; methodology, K.K.K., A.L.K., K.B.E., I.E.K. and M.V.Z.; formal analysis, K.K.K., S.N.K., A.L.K., K.B.E., I.E.K. and M.V.Z.; investigation, K.K.K., S.N.K., A.L.K., K.B.E., I.E.K. and M.V.Z.; resources, K.K.K. and A.L.K.; writing—original draft preparation, review and editing, A.L.K. and K.K.K.; visualization, K.K.K., A.L.K., K.B.E., I.E.K. and M.V.Z.; supervision, K.K.K. All authors have read and agreed to the published version of the manuscript.

Funding: This study was funded by the Ministry of Education and Science of the Republic of Kazakhstan (grant AP09259184).

Institutional Review Board Statement: Not applicable.

Informed Consent Statement: Not applicable.

Data Availability Statement: Not applicable.

Conflicts of Interest: The authors declare no conflict of interest.

References

1. Yan, C.; Qu, Z.; Wang, J.; Cao, L.; Han, Q. Microalgal bioremediation of heavy metal pollution in water: Recent advances, challenges, and prospects. *Chemosphere* **2022**, *286*, 131870. [[CrossRef](#)] [[PubMed](#)]
2. Li, H.; Watson, J.; Zhang, Y.; Lu, H.; Liu, Z. Environment-enhancing process for algal wastewater treatment, heavy metal control and hydrothermal biofuel production: A critical review. *Bioresour. Technol.* **2020**, *298*, 122421. [[CrossRef](#)] [[PubMed](#)]
3. Burakov, A.E.; Galunin, E.V.; Burakova, I.V.; Kucherovala, A.E.; Agarwal, S.; Tkachev, A.G.; Gupta, V.K. Adsorption of heavy metals on conventional and nanostructured materials for wastewater treatment purposes: A review. *Ecotoxicol. Environ. Saf.* **2018**, *148*, 702–712. [[CrossRef](#)]
4. Tripathi, A.; Ranjan, M.R. Heavy metal removal from wastewater using low cost adsorbents. *J. Bioremed. Biodeg.* **2015**, *6*, 315. [[CrossRef](#)]
5. Yaqoob, A.A.; Parveen, T.; Umar, K.; Mohamad Ibrahim, M.N. Role of nanomaterials in the treatment of wastewater: A review. *Water* **2020**, *12*, 495. [[CrossRef](#)]
6. Larsson, D.J.; Fick, J. Transparency throughout the production chain—A way to reduce pollution from the manufacturing of pharmaceuticals? *Regul. Toxicol. Pharmacol.* **2009**, *53*, 161–163. [[CrossRef](#)]
7. Rajendran, S.; Priya, A.K.; Kumar, P.S.; Hoang, T.K.; Sekar, K.; Chong, K.Y.; Show, P.L. A critical and recent developments on adsorption technique for removal of heavy metals from wastewater—A review. *Chemosphere* **2022**, *303*, 135146. [[CrossRef](#)] [[PubMed](#)]
8. Galina, S.; Strand, M.; Øye, G. Potential applications of magnetic nanoparticles within separation in the petroleum industry. *J. Pet. Sci. Eng.* **2018**, *165*, 488–495.
9. Hosain, A.N.; El Nemr, A.; El Sikaily, A.; Mahmoud, M.E.; Amira, M.F. Surface modifications of nanochitosan coated magnetic nanoparticles and their applications in Pb (II), Cu (II) and Cd (II) removal. *J. Environ. Chem. Eng.* **2020**, *8*, 104316. [[CrossRef](#)]

10. Ul-Islam, M.; Ullah, M.W.; Khan, S.; Manan, S.; Khattak, W.A.; Ahmad, W.; Park, J.K. Current advancements of magnetic nanoparticles in adsorption and degradation of organic pollutants. *Environ. Sci. Pollut. Res.* **2017**, *24*, 12713–12722. [[CrossRef](#)] [[PubMed](#)]
11. Li, X.M.; Xu, G.; Liu, Y.; He, T. Magnetic Fe₃O₄ nanoparticles: Synthesis and application in water treatment. *Nanosci. Nanotechnol. Asia* **2011**, *1*, 14–24.
12. Pang, Y.; Zeng, G.; Tang, L.; Zhang, Y.; Liu, Y.; Lei, X.; Xiong, Y. Preparation and application of stability enhanced magnetic nanoparticles for rapid removal of Cr (VI). *Chem. Eng. J.* **2011**, *175*, 222–227. [[CrossRef](#)]
13. Wei, Y.; Han, B.; Hu, X.; Lin, Y.; Wang, X.; Deng, X. Synthesis of Fe₃O₄ nanoparticles and their magnetic properties. *Procedia Eng.* **2012**, *27*, 632–637. [[CrossRef](#)]
14. Nguyen, M.D.; Tran, H.V.; Xu, S.; Lee, T.R. Fe₃O₄ nanoparticles: Structures, synthesis, magnetic properties, surface functionalization, and emerging applications. *Appl. Sci.* **2021**, *11*, 11301. [[CrossRef](#)] [[PubMed](#)]
15. El Ghandoor, H.; Zidan, H.M.; Khalil, M.M.; Ismail, M.I.M. Synthesis and some physical properties of magnetite (Fe₃O₄) nanoparticles. *Int. J. Electrochem. Sci.* **2012**, *7*, 5734–5745.
16. Sheng, P.; Sun, S. Synthesis and characterization of monodisperse hollow Fe₃O₄ nanoparticles. *Angew. Chem.* **2007**, *119*, 4233–4236.
17. Iida, H.; Takayanagi, K.; Nakanishi, T.; Osaka, T. Synthesis of Fe₃O₄ nanoparticles with various sizes and magnetic properties by controlled hydrolysis. *J. Colloid Interface Sci.* **2007**, *314*, 274–280. [[CrossRef](#)]
18. Biehl, P.; Von der Lühse, M.; Dutz, S.; Schacher, F.H. Synthesis, characterization, and applications of magnetic nanoparticles featuring polyelectrolytic coatings. *Polymers* **2018**, *10*, 91. [[CrossRef](#)]
19. Liu, S.; Yu, B.; Wang, S.; Shen, Y.; Cong, H. Preparation, surface functionalization and application of Fe₃O₄ magnetic nanoparticles. *Adv. Colloid Interface Sci.* **2020**, *281*, 102165. [[CrossRef](#)]
20. Ramos-Guivar, J.A.; Taipei, K.; Schettino, M.A., Jr.; Silva, E.; Morales Torres, M.A.; Passamani, E.C.; Litterst, F.J. Improved removal capacity and equilibrium time of maghemite nanoparticles growth in zeolite type 5A for Pb (II) adsorption. *Nanomaterials* **2020**, *10*, 1668. [[CrossRef](#)]
21. Mahmoud, M.E.; Nabil, G.M.; Zaki, M.M.; Saleh, M.M. Starch functionalization of iron oxide by-product from steel industry as a sustainable low cost nanocomposite for removal of divalent toxic metal ions from water. *Int. J. Biol. Macromol.* **2019**, *137*, 455–468. [[CrossRef](#)] [[PubMed](#)]
22. Maity, R.; Dutta, A.; Halder, S.; Shannigrahi, S.; Mandal, K.; Sinha, T.P. Enhanced photocatalytic activity, transport properties and electronic structure of Mn doped GdFeO₃ synthesized using the sol–gel process. *Phys. Chem. Chem. Phys.* **2021**, *23*, 16060–16076. [[CrossRef](#)] [[PubMed](#)]
23. Lim, D.T.; Tuyen, T.N.; Nhiem, D.N.; Duc, D.H.; Chuc, P.N.; Bac, N.Q.; Tung, D.X.; Pham, N.N.; Ha, L.T.V.; Tu, N.T.T.; et al. Fluoride and arsenite removal by adsorption on La₂O₃-CeO₂/laterite. *J. Nanomater.* **2021**, *2021*, 9991050. [[CrossRef](#)]
24. Osagie, C.; Othmani, A.; Ghosh, S.; Malloum, A.; Esfahani, Z.K.; Ahmadi, S. Dyes adsorption from aqueous media through the nanotechnology: A review. *J. Mater. Res. Technol.* **2021**, *14*, 2195–2218. [[CrossRef](#)]
25. Yagub, M.T.; Sen, T.K.; Afroze, S.; Ang, H.M. Dye and its removal from aqueous solution by adsorption: A review. *Adv. Colloid Interface Sci.* **2014**, *209*, 172–184. [[CrossRef](#)]
26. Sayan, B.; Indranil, S.; Aniruddha, M.; Dhruvajyoti, C.; Uday, C.G.; Debashis, C.J.T. Role of nanotechnology in water treatment and purification: Potential applications and implications. *Int. J. Chem. Sci. Technol.* **2013**, *3*, 59.
27. Deka, S.; Saxena, V.; Hasan, A.; Chandra, P.; Pandey, L.M. Synthesis, characterization and in vitro analysis of α -Fe₂O₃-GdFeO₃ biphasic materials as therapeutic agent for magnetic hyperthermia applications. *Mater. Sci. Eng. C* **2018**, *92*, 932–941. [[CrossRef](#)] [[PubMed](#)]
28. Gonzalo, A.L.; Cecilia, F.S.; Inés, G.M.; Marcela, F.; Adriana, S.; Cintia, M.R.; Carolina, N.M. Bioremediation of arsenic using magnetic NdFeO₃ nanoparticles functionalized with microbial biofilm. *J. Environ. Chem. Eng.* **2023**, *11*, 109532.
29. Sepideh, B.; Anbia, M.; Salehi, S. Comparison of MnO₂ modified and unmodified magnetic Fe₃O₄ nanoparticle adsorbents and their potential to remove iron and manganese from aqueous media. *J. Alloys Compd.* **2021**, *851*, 156822.
30. Liliana, G.; Erto, A.; Moreno-Piraján, J.C. Magnetite nanoparticles for removal of heavy metals from aqueous solutions: Synthesis and characterization. *Adsorption* **2013**, *19*, 465–474.
31. Ghobadi, M.; Gharabaghi, M.; Abdollahi, H.; Kisomi, A.S. A simple and low-cost route to recycle rare earth elements (La, Ce) from aqueous solution using magnetic nanoparticles of Co_xMn_{1-x}Fe₂O₄ (x = 0.2 and 0.8): Synthesis, isotherms, kinetics, thermodynamics and desorption. *New J. Chem.* **2017**, *41*, 11906–11914. [[CrossRef](#)]
32. Ivanets, A.I.; Srivastava, V.; Roshchina, M.Y.; Sillanpää, M.; Prozorovich, V.G.; Pankov, V.V. Magnesium ferrite nanoparticles as a magnetic sorbent for the removal of Mn²⁺, Co²⁺, Ni²⁺ and Cu²⁺ from aqueous solution. *Ceram. Int.* **2018**, *44*, 9097–9104. [[CrossRef](#)]
33. Shekari, H.; Sayadi, M.H.; Rezaei, M.R.; Allahresani, A. Synthesis of nickel ferrite/titanium oxide magnetic nanocomposite and its use to remove hexavalent chromium from aqueous solutions. *Surf. Interfaces* **2017**, *8*, 199–205. [[CrossRef](#)]

Disclaimer/Publisher's Note: The statements, opinions and data contained in all publications are solely those of the individual author(s) and contributor(s) and not of MDPI and/or the editor(s). MDPI and/or the editor(s) disclaim responsibility for any injury to people or property resulting from any ideas, methods, instructions or products referred to in the content.